Electron paramagnetic resonance of $Zn_{1-x}Mn_xO$ thin films and single crystals

Mariana Diaconu,* Heidemarie Schmidt, Andreas Pöppl, Rolf Böttcher, Joachim Hoentsch, Alexander Klunker, Daniel Spemann, Holger Hochmuth, Michael Lorenz, and Marius Grundmann
Institut für Experimentelle Physik II, Fakultät für Physik und Geowissenschaften, Universität Leipzig, Linnéstraße 3-5, 04103 Leipzig, Germany
(Received 26 January 2005; published 16 August 2005)

X-band electron paramagnetic resonance spectra were recorded for $Zn_{1-x}Mn_xO$ films grown by pulsed laser deposition and a single crystal for comparison. For different Mn concentrations in $Zn_{1-x}Mn_xO$ films we performed measurements in dependence on the angle between the applied magnetic field and the *c* axis of the wurtzite ZnMnO lattice. The fine and hyperfine structure splitting parameters and *g* values were determined by modeling the experimental spectra. For both single crystal and films the investigations showed the incorporation of Mn ions at Zn lattice sites as Mn^{2+}. For higher Mn concentrations, a broad Lorentzian single line, probably due to divalent Mn ions in higher local concentrations undergoing exchange, was found superimposed onto the resolved Mn^{2+} spectrum at $g=2.000$. Furthermore, by extrapolating the lattice-distortion-dependent fine-structure parameters determined for samples with a Mn content of $x \leqslant 0.035$, we anticipate that for $Zn_{1-x}Mn_xO$ single crystals and thin films on *c*-plane sapphire with $x=0.045$ the *D* fine-structure parameters should be equal.

DOI: 10.1103/PhysRevB.72.085214 PACS number(s): 71.55.Gs, 76.30.Fc, 75.50.Pp, 75.30.Hx

I. INTRODUCTION

II-VI and III-V diluted magnetic semiconductors (DMS's), in which magnetic ions substitute for the cations of the host semiconducting material, are developed for spintronic technology. Such new materials that exhibit both room temperature ferromagnetism and semiconducting properties are useful for devices like spin field-effect transistors (FET's) or spin light-emitting diodes (LED's). For example, the $Zn_{1-x}Mn_xO$ system is very promising because of the wide band, gap of the ZnO host material 3.37 eV at room temperature), which is used for UV optoelectronic devices, and because of the high solubility of Mn in ZnO due to similar ionic radii (80 pm for Mn^{2+} and 74 pm for Zn^{2+}).[1] Recently, ferromagnetism has been found in $Zn_{1-x}Mn_xO$ films.[2,3] Because the origin of the observed ferromagnetism has not yet been revealed, the present paper focuses on electron paramagnetic resonance (EPR) investigations of $Zn_{1-x}Mn_xO$ in order to determine whether the Mn ions are isovalently replacing the Zn^{2+} ions in the wurtzite lattice. There have been many EPR studies of Mn impurities in ZnO ceramics, single crystals, and quantum dots.[4–9] A few EPR studies were also performed of $Zn_{1-x}Mn_xO$ thin films obtained using different growing techniques.[2,9,10] This paper is organized as follows: in Sec. II the sample preparation and EPR instrumentation are presented, in Sec. III the theoretical aspects are presented, and in Sec. IV the experimental results for $Zn_{1-x}Mn_xO$ thin films and single crystals are discussed. From the fine and hyperfine structure parameters of Mn ions in $Zn_{1-x}Mn_xO$ determined by modeling the 6-K EPR spectra we conclude that the charge state of Mn ions in the wurtzite lattice is 2+ and that the Mn^{2+} ions are incorporated at Zn lattice sites.

II. SAMPLE PREPARATION AND INSTRUMENTATION

$Zn_{1-x}Mn_xO$ films with a thickness around 1 μm have been grown on 10×10 mm^2 *c*-plane sapphire substrates by pulsed laser deposition (PLD).[11] The films crystallize in wurtzite structure and have their *c* axis perpendicular to the *c*-plane sapphire substrate (0001) surface plane. The PLD targets were sintered ceramic pellets mixed and pressed from appropriate amounts of ZnO and MnO or MnO_2 powders.

We investigated films having almost isolated Mn ions, with $x=0.001$, and also films with higher Mn contents, up to $x=0.091$, in which ferromagnetism is expected. The Mn content of the films was determined by Rutherford backscattering spectrometry (RBS) and particle induced X-ray emission (PIXE) measurements using 1.2-MeV proton beams. From PIXE [0001]-channeling experiments we found that the position of Mn ions does not deviate from the position of Zn ions when viewed along the [0001] direction.

The investigated $Zn_{1-x}Mn_xO$ single crystal was prepared by chemical transport of solid ZnO/MnO solutions with HCl as transport agent at a temperature of 650 °C.[12] Energy-dispersive x-ray (EDX) analysis measurements revealed a Mn content of $x=0.035$. The lattice parameters of this single crystal have been determined by powder x-ray diffractometry (XRD) and amount to $a=3.257$ Å and $c=5.214$ Å. The lattice parameters of the $Zn_{1-x}Mn_xO$ thin film on *c*-plane sapphire with $x=0.001$ were determined by XRD $2\theta-\omega$ scans and amount to $a=3.264$ Å and $c=5.199$ Å These values agree with the lattice parameters determined by Kim *et al.*[13] measured on ZnMnO films epitaxially grown by PLD on *c*-plane sapphire. Despite the general expansion of the *a* and *c* axis lengths with increasing Mn content in wurtzite ZnMnO single crystals, the increase of the *a* axis in epitaxial ZnMnO films on *c*-plane sapphire is marginal compared to the strong increase of the *c* axis.[13]

The EPR spectra were recorded using a Bruker ESP 380E spectrometer at *X*-band frequency with a standard TE_{102} cavity. The single crystal and film pieces with an area of 2 mm $\times$ 5 mm were mounted on a quartz rod sample holder. The angle between the *c* axis of the films and the direction of the applied magnetic field was controlled by a goniometer,

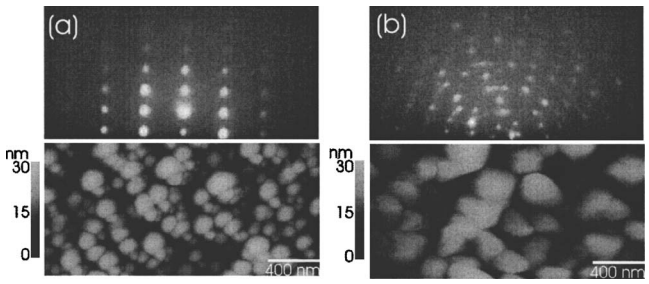

FIG. 1. RHEED (top) and AFM (bottom) results for an epitaxial (a) and a textured (b) $Zn_{1-x}Mn_xO$ film with $x=0.001$ grown at 0.3 mbar and 550 °C (a) and 430 °C (b), respectively.

and the strength of the magnetic field was varied between 1 kG and 6 kG, while the microwave frequency has been kept constant at 9.5 GHz.

The films were analyzed with respect to surface roughness and grain formation by atomic force microscopy (AFM) using a Dimension 3100 scanning probe microscope. The average surface roughness was less than 20 nm for all films, while the grain size for different samples varied between 60 nm and 250 nm. Information about the crystalline quality of the films was obtained by reflection high-energy electron diffraction (RHEED) measurements using an EK-2035-R electron gun. An epitaxial material, with well-aligned grains and high structural quality, will give rise to a "spotty" RHEED pattern, whereas already a small distribution of orientations will give rise to a "textured" RHEED pattern, consisting of concentric broken rings or arcs. The length of these arcs is a measure for the misorientation of the grains.[14] In Fig. 1 the RHEED patterns and AFM images of two $Zn_{1-x}Mn_xO$ films, both having $x=0.001$, grown at the same oxygen pressure, 0.3 mbar, but at different temperatures, are represented. The film grown at 550 °C reveals an epitaxial surface structure in its spotty RHEED pattern [Fig. 1(a)], whereas the surface structure of the film grown at 430 °C is textured and reveals a small tilting of the grains with respect to the c axis [Fig. 1(b)]. In Sec. IV the influence of the structural properties of the films on the EPR spectra will be discussed.

III. THEORY

The electronic configuration of Mn^{2+} ions is $3d^5$, and the electronic ground state of free ions is $^6S_{5/2}$. The spin Hamiltonian of the Mn^{2+} ion, with the electron spin $S=5/2$ and the nuclear spin $I=5/2$ for the ^{55}Mn isotope, can be written[4]

$$\mathcal{H} = \mu_B \vec{S} g \vec{B} + D\left[S_z^2 - \frac{1}{3}S(S+1)\right] + \frac{7F}{36}\left[S_z^4 - \frac{95}{14}S_z^2 + \frac{81}{16}\right] + \frac{a}{6}\left[(S_{x'}^4 + S_{y'}^4 + S_{z'}^4) + \frac{1}{5}S(S+1)(3S^2+3S-1)\right] + \vec{S}A\vec{I}, \quad (1)$$

where g is the electron g-factor tensor, D and F are the axial fine-structure parameters, a is the cubic fine-structure parameter, and A is the hyperfine-structure parameter tensor. The first term of the equation is the electron Zeeman term; the second and third terms are due to the axial zero-field splitting, caused by a trigonal distortion of the $Mn\text{-}O_4$ tetrahedron along the c axis of the crystal. The last term is the electron-nuclear magnetic hyperfine coupling term. The (x,y,z) coordinates refer to the trigonal axes of the crystal field, while the (x',y',z') coordinates refer to the cubic axes of the crystal field.[15]

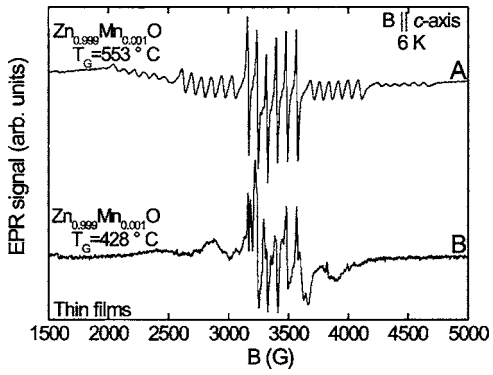

FIG. 2. Experimental spectra at 6 K and $\mathbf{B}\|c$ axis for $Zn_{1-x}Mn_xO$ films with $x=0.001$, grown at 0.3 mbar and 550 °C (A) and 430 °C (B), respectively. Five ($2S$) groups of six ($2I+1$) hyperfine lines confirm the incorporation of ^{55}Mn as Mn^{2+} in $Zn_{1-x}Mn_xO$ thin films.

In a magnetic field the spin degeneracy of Mn^{2+} will be lifted by the Zeeman splitting, resulting in six energy levels classified by magnetic electron spin quantum number M_S. Due to hyperfine splitting, each of these transitions will be split into six hyperfine sublevels characterized by the magnetic nuclear spin quantum number M_I.[4,6]

The experimental spectra of $Zn_{1-x}Mn_xO$ films and single crystal were modeled by exact diagonalization of the spin Hamiltonian [Eq. (1)] using the Easy Spin MATLAB toolbox.[16,17] We may notice that the main hyperfine lines in the spectra are due to allowed $\Delta M_S=\pm 1$ transitions with $\Delta M_I=0$, while also other lines from forbidden transitions, with nonzero ΔM_I, may be observed in case when the external field **B** is not aligned parallel or perpendicular to the c axis.

IV. EXPERIMENTAL RESULTS AND DISCUSSION

Using X-band EPR spectroscopy at 6 K we probed the valence of the incorporated Mn ions in $Zn_{1-x}Mn_xO$ films. The magnetic interactions between Mn ions were studied using the temperature dependence of the EPR lines.

In Fig. 2 we compare the EPR spectra for two $Zn_{1-x}Mn_xO$ films with $x=0.001$: one epitaxial and one textured. We observed that the crystalline quality of the films (Fig. 1) influences the EPR spectra (Fig. 2). For the epitaxial film the typical Mn^{2+} ($S=5/2$, $I=5/2$) spectrum with 30 lines, five fine-structure transitions each split into six hyperfine lines, is observed. For the textured film the hyperfine lines were only observed for the central $M_S=1/2\leftrightarrow -1/2$ transition. In addition to the typical sextet of allowed $\Delta M_I=0$ transitions, some intense forbidden transitions with $\Delta M_I=\pm 1$ are observed,

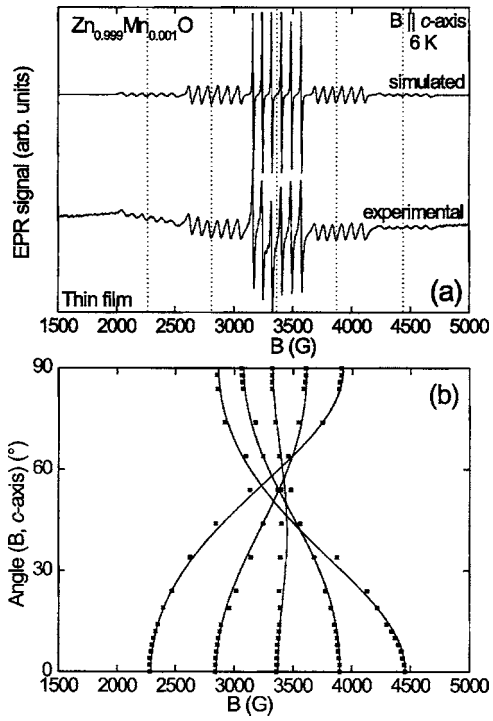

FIG. 3. (a) Simulated and experimental spectra at 6 K for $\mathbf{B}\|c$ axis for a $Zn_{1-x}Mn_xO$ film with $x=0.001$ grown at 550 °C and 0.3 mbar. (b) Angular dependence of the fine-structure transitions. The experimental results are represented as points and the lines are simulated. It can be seen that the maximum separation between the outermost lines is obtained for $\mathbf{B}\|c$ axis.

indicating a disorder of c-axis orientations of the grains with respect to the normal on the sapphire substrate. The presence of such grains is supported by the RHEED pattern of the textured film [Fig. 1(b)]. The sextets of the other fine-structure transitions, $\Delta M_S=\pm 5/2\leftrightarrow\pm 3/2$, $\pm 3/2\leftrightarrow\pm 1/2$, were seriously broadened so that the hyperfine structure is not resolved.

The epitaxial film with $x=0.001$, where all 30 lines typical for isolated Mn^{2+} ions have been observed, was studied in detail to determine the fine- and hyperfine-structure parameters. For determining the anisotropy of the g and A tensors, we took into account the spectra obtained for $\mathbf{B}\perp c$ axis and for $\mathbf{B}\|c$ axis. We found that the best fit of the experimental results by Eq. (1) is obtained for isotropic g and A tensors within the experimental accuracy of the EPR spectra determined by the line widths of Mn^{2+} signals. In the $\mathbf{B}\|c$ axis spectrum [Fig. 3(a)] we observe that the low-field fine structure lines are more intense than the high-field lines, meaning a negative D value in Eq. (1). As expected, for the transitions $M_S=\pm 3/2\leftrightarrow\pm 1/2$, half of the lines are shifted by $2D$ to higher fields and the other half by $2D$ to lower fields, while for the transitions $M_S=\pm 5/2\leftrightarrow\pm 3/2$ the shift is with $4D$. We did not obtain the theoretically predicted amplitude ratios of 5:8:9:8:5 of the fine-structure transitions found for Mn^{2+} in ZnO:Mn single crystals.[4] This indicates a distribution of the D fine-structure parameter. The angular dependences of the centers of gravity of the hyperfine sextets, also giving the centers of the fine-structure transitions, are plotted versus the angle between $\mathbf{B}$ and c axis. We observe that the maximum fine-structure splitting is obtained for $\mathbf{B}\|c$ axis, in accordance with the hexagonal structure of ZnO and the trigonal symmetry of Zn site.

We modeled the experimental spectrum for $\mathbf{B}\|c$ axis and determined the fine-structure parameters D and $|a-F|$. We used a Gaussian distribution of D with distribution width $\Delta D=18$ MHz for taking into account the experimentally observed amplitude ratio of the fine-structure transitions presumably caused by small structural distortions in films. The determined spin-Hamiltonian parameters are listed in Table I. Using these parameters, the angular dependence of the fine-structure transitions could be nicely reproduced [Fig. 3(b)].

We noticed that for samples with higher Mn content, $x\geqslant 0.017$, due to dipolar broadening, the hyperfine structure is not visible anymore. Furthermore, the Mn^{2+} fine-structure lines are superimposed by a broad isotropic single line at about $g=2.000$ [Fig. 4(a)]. In order to simulate the experimental $\mathbf{B}\|c$ axis spectra for $x\geqslant 0.017$, the parameters g, A, and $|a-F|$ were taken from the high-quality film with a low Mn content of $x=0.001$. In order to account for broadening effect of the Mn^{2+} fine-structure lines, the computed Mn^{2+} spectrum was convoluted by a Lorentzian line with a line-

TABLE I. Parameters from modeling experimental spectra recorded at 6 K for $Zn_{1-x}Mn_xO$ thin films and a single crystal. We also included the single-crystal parameters determined by Hausmann and Huppertz (Ref. 4).

	Mn^{2+} spectrum					Broad single line	
Mn content (x)	g	A (MHz)	D (MHz)	ΔD (MHz)	$\lvert a-F\rvert$ (MHz)	g	ΔB (MHz)
Thin film							
0.001	$2.0012\pm 4\times 10^{-4}$	-225 ± 5	-757 ± 15	18	16.5		
0.017	$2.0012\pm 4\times 10^{-4}$	-225 ± 10	-715 ± 30	25	16.5	$2.000\pm 3\times 10^{-3}$	910 ± 30
0.028	$2.0012\pm 4\times 10^{-4}$	-225 ± 10	-690 ± 30	25	16.5	$2.000\pm 3\times 10^{-3}$	1078 ± 30
0.091						$2.000\pm 3\times 10^{-3}$	1230 ± 30
Single crystal							
<0.001[a]	$1.9984\pm 2\times 10^{-4}$[a]	-222[a]	-706[a]		16.3[a]		
0.035	$2.0012\pm 1\times 10^{-4}$	-220 ± 10	-675 ± 30	20	16.5	$2.000\pm 3\times 10^{-3}$	1260 ± 30

[a]Reference 4.

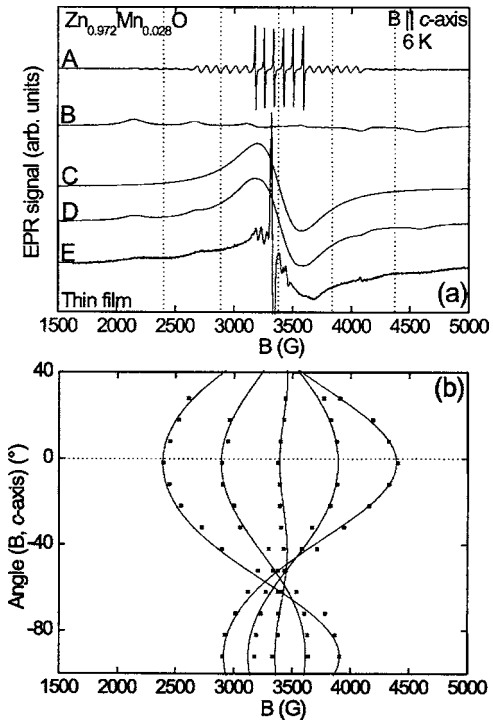

FIG. 4. (a) Simulated and experimental spectra at 6 K for $\mathbf{B}\|c$ axis for a $Zn_{1-x}Mn_xO$ film with $x=0.028$, grown at 298 °C and 0.3 mbar. *A* is the typical Mn^{2+} spectrum, *B* is the Mn^{2+} spectrum (*A*) broadened by dipole-dipole interactions, *C* is the broad isotropic Lorentzian line probably due to Mn ions in higher local concentrations, *D* is the simulated spectrum ($B+C$), and *E* is the experimental spectrum. The sharp intense lines in the experimental spectrum at 3200–3500 G are caused by a paramagnetic impurity of the substrate. (b) Angular dependence of the fine-structure transitions, the dotted line indicates $\mathbf{B}\|c$ axis. Points represent experimental data and solid lines are results of the simulations. The angular dependence behavior is characteristic for Mn^{2+} fine-structure lines.

width of 336 MHz. Furthermore, the resulting spectrum was superimposed by a broad Lorentzian single line. The simulation procedure is shown in Fig. 4(a) for $x=0.028$. Finally, the angular dependence of the Mn^{2+} fine-structure splitting was modeled with the obtained parameters g, D, and $|a-F|$, to verify spectral analysis. As an example, calculated and experimental angular dependences of fine-structure lines for $x=0.028$ are presented in Fig. 4(b). Again, maximal fine-structure splitting is observed for $\mathbf{B}\|c$ axis in accordance with the trigonal symmetry of the Mn site. In the same manner, the EPR spectra from the samples with $x=0.017$ and $x=0.091$ (Fig. 5) have been analyzed.

In order to support the analysis of films with higher Mn content, a $Zn_{1-x}Mn_xO$ single crystal with $x=0.035$ was also studied. Experimental and simulated spectra for $\mathbf{B}\|c$ axis and angular dependence of fine-structure transitions are presented in Fig. 6. We observed again the dipolar broadening of the lines, leading to the loss of the hyperfine-structure lines of Mn^{2+} and the superposition of a broad isotropic single line with $g=2.000$. The angular dependence of the fine-structure transitions displays the behavior expected for Mn^{2+} in trigonal Zn lattice sites, with maximum splitting for $\mathbf{B}\|c$ axis.

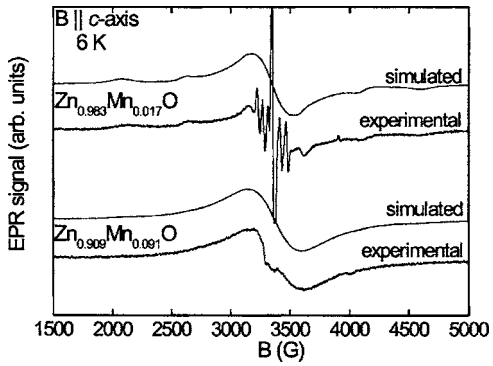

FIG. 5. Simulated and experimental EPR spectra at 6 K for $Zn_{1-x}Mn_xO$ films with $x=0.017$ and $x=0.091$. It can be observed that the Mn^{2+} fine-structure lines are not visible anymore for the $Zn_{1-x}Mn_xO$ film with $x=0.091$, and therefore only the parameters of the broad single line could be determined.

The overall features of the EPR spectrum of the single crystal (Fig. 6) are similar to those of films with $x \geqslant 0.017$ (Figs. 3 and 5).

The parameters obtained from simulated spectra for different Mn contents in $Zn_{1-x}Mn_xO$ films and from the $Zn_{0.965}Mn_{0.035}O$ single crystal are summarized in Table I.

The isotropic linewidth for taking into account the broadening of the Mn^{2+} lines by dipolar interactions was 336 MHz in all cases. The parameters obtained for wurtzite $Zn_{1-x}Mn_xO$ thin films (Table I) agree with those obtained for ZnO:Mn single crystals[4,5] and together with the fact that the maximum splitting of the fine-structure transitions was al-

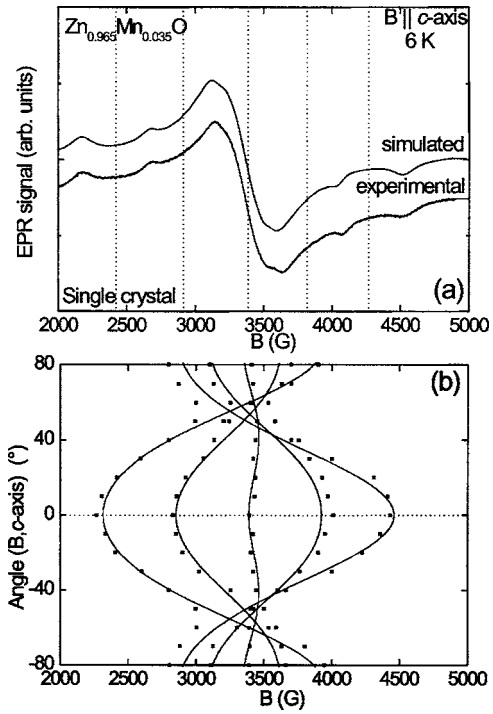

FIG. 6. (a) Simulated and experimental spectra at 6 K for $\mathbf{B}\|c$ axis for a $Zn_{1-x}Mn_xO$ single crystal with $x=0.035$. (b) Angular dependence of the fine-structure transitions; points represent experimental data and lines are results of the simulations.

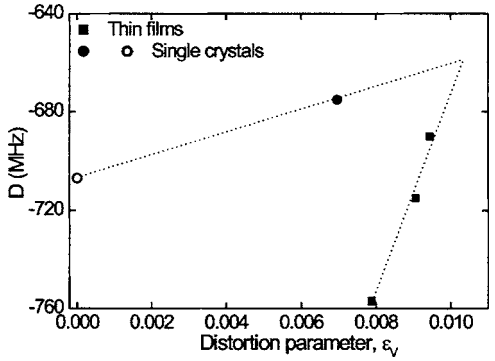

FIG. 7. Fine-structure parameter D of ZnMnO as a function of the distortion parameter ε_V for single crystals (solid circle, this work; open circle from Ref. 4) and films (squares).

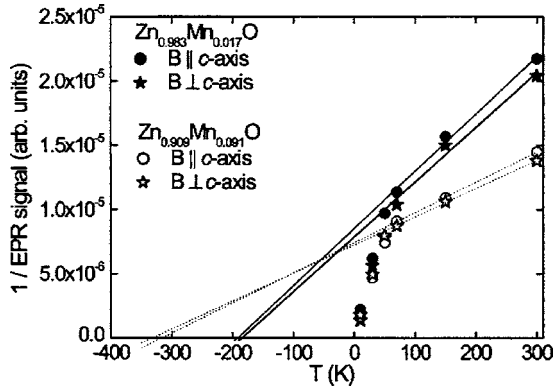

FIG. 8. Temperature dependence of the EPR intensity for the broad single Lorentzian line, indicating the presence of antiferromagnetic coupling. Points represent experimental values, while lines represent high-temperature range fitting using Eq. (4).

ways found for $\mathbf{B}\|c$ axis, meaning that the z axis of the trigonal crystal field at the Mn^{2+} site is parallel to the hexagonal c axis, are a proof that the Mn ions are incorporated at Zn lattice sites as Mn. Hausmann and Huppertz[4] determined a fine-structure parameter of $|D|=706$ MHz for a $Zn_{1-x}Mn_xO$ single crystal with $x<0.001$. For the good-quality $Zn_{0.999}Mn_{0.001}O$ film we determined $|D|=757$ MHz. This might indicate a different trigonal distortion of the $Mn\text{-}O_4$ tetrahedron even for very small Mn contents in ZnMnO thin films. With increasing Mn content we observed a decrease in the absolute value of D (Table I). The same effect can also be observed for the single crystal. This indicates that the local structure of the films and crystals at the Mn sites is also influenced by the Mn content itself.

For discussing the D fine-structure parameters, we introduce the parameter ε_V:

$$\varepsilon_V = \frac{a^2c - a_0^2c_0}{a_0^2c_0}, \tag{2}$$

which accounts for the distortion of the hexagonal lattice in single crystals and epitaxially grown thin films, where $a_0=0.3249$ nm and $c_0=0.5206$ nm are the values of the lattice parameters for undoped ZnO single crystals (JCPDS card No. 36-1451) and a and c are the lattice parameters of the specific samples. In Fig. 7 the values of the fine-structure parameter D are represented as a function of the distortion parameter. The distortion parameter ε_V of $Zn_{1-x}Mn_xO$ single crystals and epitaxially grown thin films with the same Mn content is different. In single crystals the a- and c-axis lengths increase with increasing Mn content, while in thin films, due to the epitaxial growth, only the c axis increases significantly with increasing Mn content.

The D axial fine-structure parameter of Mn^{2+} ions in $Zn_{1-x}Mn_xO$ is strongly correlated with the macroscopic strain. Using the dependence of the a and c lattice parameters on x in $Zn_{1-x}Mn_xO$ films grown on c-plane sapphire substrates,[13] we estimate that the fine-structure parameter D would be the same for $Zn_{0.955}Mn_{0.045}O$ single crystals and thin films (Fig. 7). That indicates that for $x=0.045$ the biaxial strain in $Zn_{1-x}Mn_xO$ thin films induced by the underlying c-plane sapphire substrate is close to zero. The absolute value of the fine-structure parameter decreases by 67 MHz with the Mn content increasing from $x=0.001$ to $x=0.028$. This corresponds to a decrease of the x-dependent biaxial compression $\epsilon_a(\%)=(a-a_0)/a_0$ from $\epsilon_a=+0.46\%$ to $+0.24\%$, where a and a_0 are the in-plane lattice constants of the $Zn_{1-x}Mn_xO$ films and bulk, respectively. Also in GaMnN films with the biaxial compression decreasing from $\epsilon_a=-0.25\%$ to -0.04% the absolute value of D decreases by 55 MHz.[18] Such similarities for the strain dependence of the fine-structure parameter D of Mn^{2+} ions in GaN and in ZnO are expected with respect to similar Pauling's covalency parameter. Kim *et al.*[13] observed that $Zn_{1-x}Mn_xO$ thin films on c-plane sapphire with $x=0.05$ possess a high crystalline quality; i.e., the $Zn_{0.95}Mn_{0.05}O$ films consist of a single domain rotated in-plane by 30° with respect to the substrate and ideally approach the crystalline quality of single crystals, the result supporting our findings.

The broad single line superposed onto the resolved Mn^{2+} lines, as detected in $Zn_{1-x}Mn_xO$ samples with $x\geqslant 0.017$ (Figs. 4–6), can be associated with Mn^{2+} ions in higher local concentrations undergoing exchange. The peak-to-peak width (ΔB) of this broad single line is given, for an infinite temperature, by the equation[19]

$$\Delta B_\infty = 22/\gamma[\gamma^4\hbar^2/r^6](\hbar/J)[x/(x+0.07)^{1/2}], \tag{3}$$

where r is the distance between two nearest-neighbor Mn^{2+} ions and J is the exchange integral. Both r and J are increasing with increasing Mn content x, and the peak-to-peak width of the broad single line is finally established by competing dipolar and exchange interactions.

We performed further studies in order to determine the type of interactions involved in our system. We analyzed the temperature dependence of the broad single-line intensity (Fig. 8) and we fitted the high-temperature range using a Curie-Weiss equation:

$$\text{EPR intensity} = C/(T-\theta). \tag{4}$$

Evaluating the line intensity by double integration of the EPR spectrum, we obtained $\theta=-190$ K for $x=0.017$ and $\theta=-322$ K for $x=0.091$, indicating an antiferromagnetic coupling between the magnetic ions. These experimental values

differ from the theoretical predictions stating that θ should depend on Mn concentration as[20]

$$\theta(x) = \theta_0 x. \quad (5)$$

The difference probably appears because the local concentration of the Mn ions giving the broad single line is higher than the Mn content determined by RBS and PIXE. As observed in Fig. 8 from results obtained for different orientations between the magnetic field and the *c* axis, no important magnetic anisotropy is present. Similar results have been obtained by Chikoidze *et al.*[10] for broad single lines they detected in $Zn_{1-x}Mn_xO$ films. We would also like to point out that for the low-doped samples, with $x=0.001$, we obtained a linear dependence of the inverse EPR intensity as a function of temperature, following a Curie law, as expected for isolated paramagnetic ions (not shown here).

Such a Lorentzian broad single line has no link with complex spectra obtained for Mn aggregates like dimers, trimers, and so on,[21] remarkably in agreement with the study of Jain and Upreti.[22] We would also like to point out that for $Zn_{1-x}Mn_xO$ thin films obtained from chemically synthesized nanocrystals, a much broader single line has been observed, having a *g* factor different than 2,[9] and probably has a different origin than the Lorentzian broad single line observed in our EPR spectra.

V. CONCLUSIONS AND OUTLOOK

We used the PLD technique to grow $Zn_{1-x}Mn_xO$ thin films and performed EPR measurements to prove the incorporation of Mn^{2+} ions in Zn lattice sites.

The characteristic EPR spectrum of Mn^{2+} with resolved hyperfine structure could be observed for films with a Mn content of $x=0.001$ at 6 K. The dipolar interactions between Mn ions produce a broadening of the EPR lines for higher Mn content. We could establish a connection between the EPR spectra and the crystallinity of the thin films, the spectrum from an epitaxial film showing all 30 hyperfine lines typical for Mn^{2+}, while the spectrum from a textured film did not reveal most of these lines.

The *g* and *A* tensors were found to be isotropic. The values of *D* are negative and in a range expected for Mn^{2+} incorporated at Zn^{2+} lattice sites in the ZnO wurtzite lattice. A broad single line found superposed onto the spectrum of isolated Mn^{2+} ions may be ascribed to Mn^{2+} ions in higher local concentrations undergoing exchange.

It would be of interest to investigate the distortion-dependent fine- and hyperfine-structure parameters as well as the peak-to-peak width of the Lorentzian single line as a function of Mn content for $Zn_{1-x}Mn_xO$ thin films grown on other substrates—for example, ZnO, GaN, or *r*-plane sapphire.

ACKNOWLEDGMENTS

This work has been supported (M.D., H.S., and H.H.) by the Bundesministerium für Bildung und Forschung in the framework of the Young Scientist's group "Nano-Spinelectronics" (Grant No. FKZ 03N8708) and (A.K.) by the Wilhelm-Ostwald-Schule, Willi-Bredel-Strasse 15, 04279 Leipzig. We are grateful to Gabriele Ramm for preparing the PLD targets. We thank Sonja Locmelis for growing the ZnMnO single crystal, Andreas Rahm for determining the film lattice parameters, and Nikolai Sobolev for fruitful discussions.

*Electronic address: diaconumary@yahoo.com

[1] R. D. Shannon, Acta Crystallogr., Sect. A: Cryst. Phys., Diffr., Theor. Gen. Crystallogr. **32**, 751 (1976).
[2] P. Sharma, A. Gupta, K. V. Rao, F. J. Owens, R. Sharma, R. Ahuja, J. M. Osorio Guillen, B. Johansson, and G. A. Gehring, Nat. Mater. **2**, 673 (2003).
[3] M. Diaconu, H. Schmidt, H. Hochmuth, M. Lorenz, G. Benndorf, J. Lenzner, D. Spemann, A. Setzer, K. W. Nielsen, P. Esquinazi, and M. Grundmann, Thin Solid Films **486**, 117 (2005).
[4] A. Hausmann and H. Huppertz, J. Phys. Chem. Solids **29**, 1369 (1968).
[5] J. Schneider and S. R. Sircar, Z. Naturforsch. A **17**, 570 (1962).
[6] P. Dorain, Phys. Rev. **112**, 1058 (1958).
[7] H. Zhou, D. M. Hofmann, A. Hofstaetter, and B. K. Meyer, J. Appl. Phys. **94**, 1965 (2003).
[8] G. Völkel, A. Pöppl, and B. Voigtsberger, Phys. Status Solidi A **109**, 295 (1988).
[9] N. S. Norberg, K. R. Kittilstved, J. E. Amonette, R. K. Kukkadapu, D. A. Schwartz, and D. Gamelin, J. Am. Chem. Soc. **126**, 9387 (2004).
[10] E. Chikoidze, H. J. von Bardeleben, Y. Dumont, P. Galtier, and J. L. Cantin, J. Appl. Phys. **97**, 10D316 (2005).
[11] M. Lorenz, E. M. Kaidashev, H. von Wenckstern, V. Riede, C. Bundesmann, D. Spemann, G. Benndorf, H. Hochmuth, A. Rahm, H. C. Semmelhack, and M. Grundmann, Solid-State Electron. **47**, 2205 (2003).
[12] S. Locmelis, Ph.D. thesis, Universität Hannover, 1998.
[13] S. S. Kim, J. H. Moon, B. T. Lee, O. S. Song, and J. H. Je, J. Appl. Phys. **95**, 454 (2004).
[14] D. Litvinov, T. O'Donnell, and R. Clarke, J. Appl. Phys. **85**, 2151 (1999).
[15] W. M. Walsh and L. W. Rupp, Phys. Rev. **126**, 952 (1962).
[16] S. Stoll, Ph.D. thesis, ETH Zürich, 2003.
[17] S. Stoll, IES EPR Newsletter **13** (1,2), 22 (2003).
[18] T. Graf, M. Gjukic, M. Hermann, M. S. Brandt, M. Stutzmann, and O. Ambacher, Phys. Rev. B **67**, 165215 (2003).
[19] N. Samarth and J. K. Furdyna, Phys. Rev. B **37**, 9227 (1988).
[20] J. Spalek, A. Lewicki, Z. Tarnawski, J. K. Furdyna, R. R. Galazka, and Z. Obuszko, Phys. Rev. B **33**, 3407 (1986).
[21] A. Bencini and D. Gatteschi, *EPR of Exchanged Coupled Systems* (Springer-Verlag, Berlin, 1990).
[22] A. K. Jain and G. C. Upreti, J. Phys. C **14**, 439 (1981).